Proceedings of the 21st ICSMGE, Vienna, Austria, 14 – 19 June 2026. Pistrol, Adam & Schweiger (eds.)
Published by: ÖGG, Austrian Society for Geomechanics, Salzburg, Austria, ISBN 978-3-9503898-4-5
https://doi.org/10.53243/ICSMGE2026-2325

Seismic observation of piled raft foundation supporting 36 story building mechanically connected with grid-form deep mixing walls

Junji Hamada
Takenaka R&D Institute, Takenaka Corporation, Japan, hamada.junji@takenaka.co.jp

Kenji Umemura
Nagoya Branch Office Design Department, Takenaka Corporation, Japan

Tsuyoshi Honda
Takenaka R&D Institute, Takenaka Corporation, Japan

ABSTRACT: This study describes the seismic behavior of a piled raft foundation supporting a 36-story high-rise building. The foundation combines piles and rafts, mechanically connected with grid-form ground improvement to prevent liquefaction. The observations focus on the 2024 Noto Peninsula Earthquake (M7.6) in 2024 and the Eastern Aichi Prefecture Earthquake (M5.0) in 2018. Settlement, axial force of piles, earth pressure, and water pressure beneath raft were measured. The measured results show that during distant earthquakes, the foundation's behavior was similar to the ground surface with no input loss, while nearby earthquakes exhibited significant input loss. The rotation of the foundation due to the building's rocking motion significantly affected the pile's head bending moment. The vertical load sharing ratio between the piles and the raft during earthquakes was consistent with that seen in the construction phase.

KEYWORDS: piled raft foundation, seismic observation, ground improvement, earth pressure, axial force.

1 INTRODUCTION

The piled raft foundation, which supports building loads with piles and rafts, has been applied to many buildings, including high-rise structures, due to its rationality. Long-term monitoring of settlement of the foundation has been carried out. However, seismic behavior has been studied through model experiments and numerical analyses, with limited seismic observation cases confirming the validity of earthquake-resistant design (Yamashita et al. 2012). This paper introduces seismic observation cases of a piled raft foundation supporting a 36-story high-rise building. The response acceleration of the building and input loss to the foundation are discussed, focusing

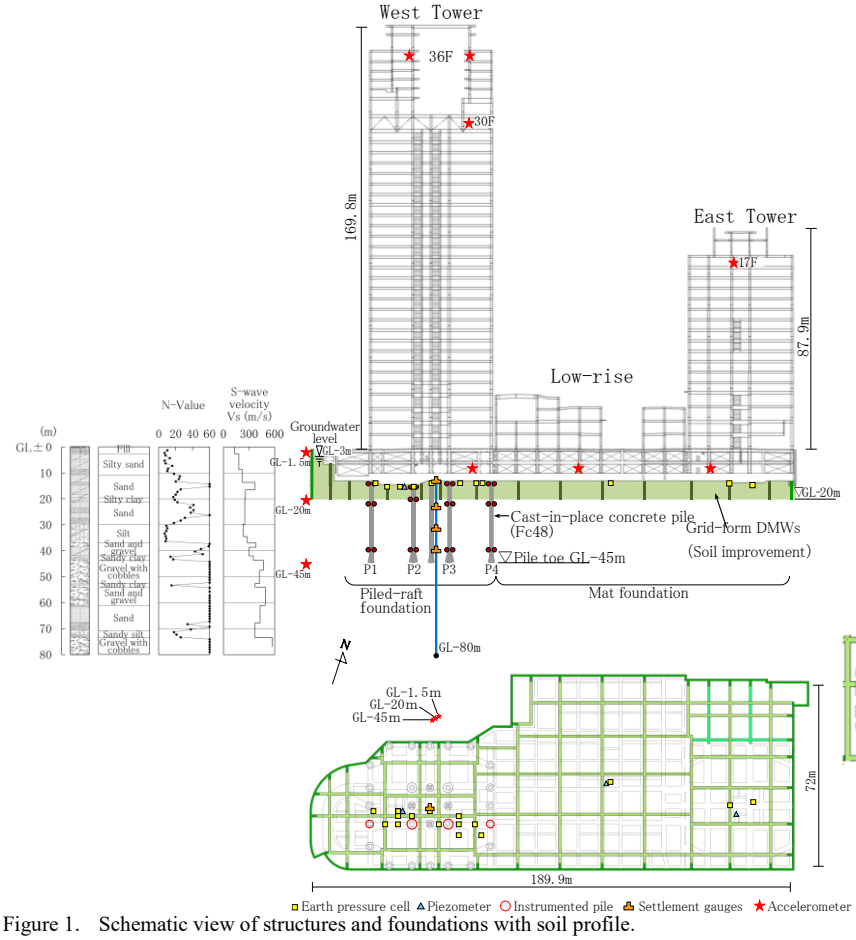

Figure 1. Schematic view of structures and foundations with soil profile.

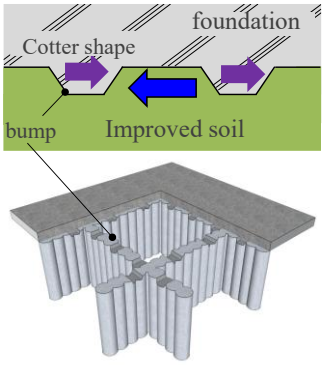

Figure 2. Mechanical joint for transmitting lateral loads to Grid-form DMWs.

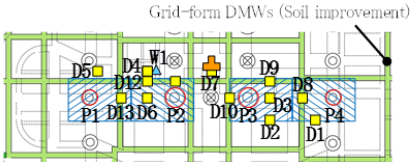

Figure 3. Locations of monitoring devices.

on the Noto Peninsula Earthquake (M7.6) on January 1, 2024, and the Eastern Aichi Prefecture Earthquake (M5.0) on October 7, 2018. The Noto Peninsula Earthquake occurred far from the observation site, whereas the Eastern Aichi Prefecture Earthquake occurred in the vicinity of the site. Seismic observation records of the foundation, such as pile strain and earth pressure beneath the raft, are analyzed to show the validity of the intended seismic design as a piled raft foundation.

2 BUILDING AND SOIL CONDITIONS

Figure 1 illustrates the layout of the building and soil conditions. The observation building comprises three interconnected structures: the West Tower (WT; 36 floors above ground, 2 basement levels), the Low-rise Building (LB; 5 floors above ground, 2 basement levels), and the East Tower (ET; 17 floors above ground, 2 basement levels). These structures are connected through their foundations.

The WT is supported by a piled raft foundation in combination with grid-form ground improvement using Deep Mixing Walls (DMWs). The base of the foundation rests on a sand layer with an N-value ranging from approximately 10 to 60. The DMWs extend to a depth of GL-20 m and are designed to support the building load (total building load: 1169 MN; average contact pressure: 421 kPa) and to mitigate liquefaction, even during extremely rare seismic events.

Cast-in-place concrete piles (shaft diameter: 1.6 to 1.9 m; tip diameter: 3.0 to 3.8 m), which are fixed into a gravel layer deeper than GL-43.7 m, are used to reduce settlement. Additionally, the DMWs resist horizontal loads and help to prevent torsional deformation among the three buildings (WT, LB, and ET), thereby reducing stress on the piles during earthquakes. To prevent foundation sliding due to buoyancy at the groundwater level (GL-3.0 m), the DMWs and raft foundation are mechanically connected (Figure 2) (Tanikawa et al., 2015).

The ground consists of medium sand with gravel (fine sand layer) from the foundation bottom to GL-19.7 m, with an N-value of approximately 10 to 60 and a shear wave velocity (Vs) of about 220 to 370 m/s. Below this, from GL-19.7 to 29.8 m, there is a sand layer with an N-value of 20 or more and Vs of approximately 250 m/s. Further below, from GL-29.8 to 34.6 m, sandy silt and clayey silt layers are present, with an N-value of around 10 and Vs of about 230 m/s. Beneath these layers lies a gravel layer, and below GL-43.7 m, a cobble layer with Vs over 400 m/s is distributed.

3 LONG TERM STATICALLY MONITORING

Figures 1 and 3 show the measurement locations. Pairs of LVDT-type strain gauges were installed at three depths (GL-13.4m, -21.3 m and -39.3 m) on four piles: P2 and P3 (shaft diameter: 1.9 m), and P1 and P4 (1.6 m). In addition, 13 earth pressure gauges and one water pressure gauge were installed at GL-12.8m beneath the raft, near the instrumented piles. To measure ground subsidence, differential settlement gauges were installed at four depths (GL-14.0m, -25.0 m, -35.0 m, -45.0 m), with a reference point at GL-80.0m.

Figure 4 shows the measured ground settlement over time following rebound due to excavation. After the ground at GL-

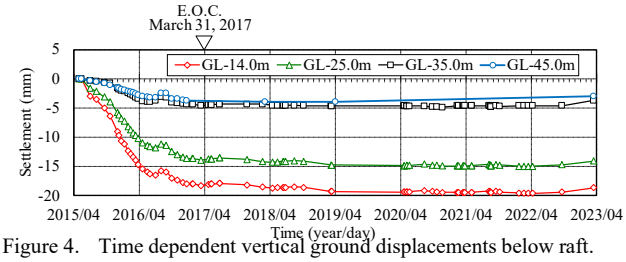

Figure 4. Time dependent vertical ground displacements below raft.

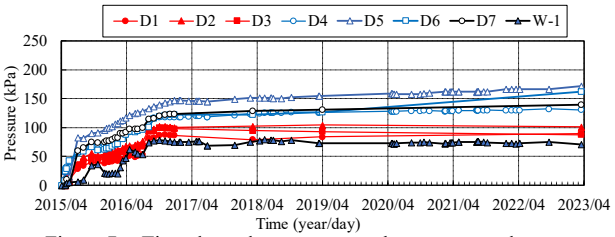

Figure 7. Time dependent contact earth pressures and porewater pressure (Original soil).

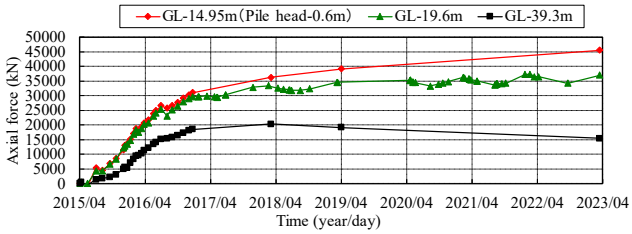

Figure 5. Time dependent axial loads of pile P2.

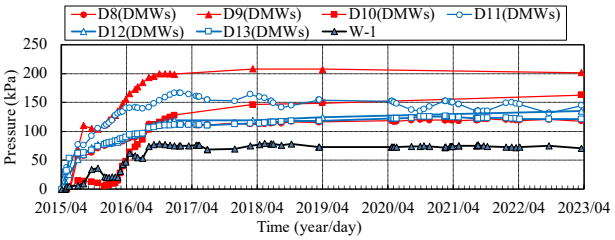

Figure 8. Time dependent contact earth pressures and porewater pressure (DMWs).

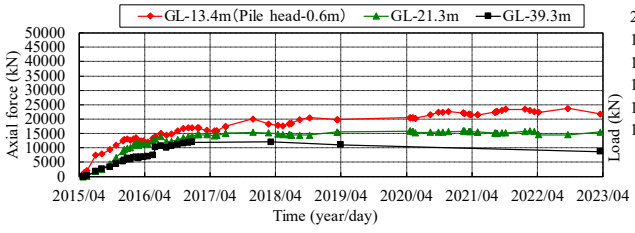

Figure 6. Time dependent axial loads of pile P4.

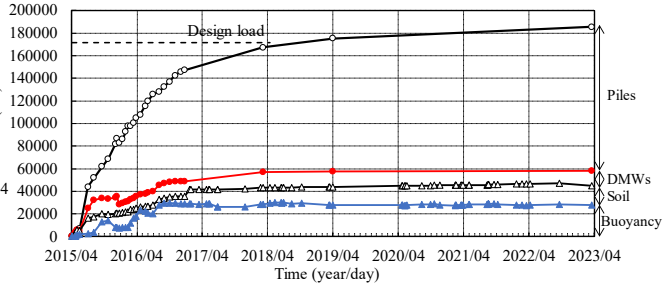

Figure 9. Time dependent load sharing among piles, DMWs and soil in the tributary area.

14.0 m rebounded by 17 mm, the settlement reached 18.3 mm at the end of construction (E.O.C.) and 19.4 mm six years after E.O.C. Figures 5 and 6 show the piles' axial force over time. The pile head axial force (pile head -0.6 m) at the E.O.C. was 31 MN for P2 and 15.8 MN for P4. Six years after the E.O.C., it was 45.5 MN for P2 and 21.8 MN for P4, and both of them were increasing. The pile axial force is calculated by assuming that the Young's modulus of concrete, Ec, is 2.98×10^7 kN/m^2 (Fc = 48 N/mm^2) and that of reinforcing steel, E is 2.05×10^8 kN/m^2 is taken into account. Figures 7 and 8 show the earth pressures and water pressure beneath the raft over time. Six years after the E.O.C., the earth pressures at the Deep Mixing Walls (DMWs) ranged from 122 to 201 kPa, while those of the original ground ranged from 90 to 172 kPa. Although the pressures showed a slight increase, they remained stable.

Figure 9 shows the load sharing among piles, DMWs and soil within the tributary area. The axial forces of the piles P1 and P3 are indicated at GL-21.3m instead of at the pile head, due to the instrument malfunction. The tributary area was 388.8m^2 in total: 66.2m^2 for the DMWs, 312.9m^2 for the original ground, and 9.7m^2 for the piles. The load supported by the raft was calculated by multiplying each area by the measured earth pressure. The used earth pressure of the DMWs was D9 (final 201 kPa), which showed the most reliable response, and the earth pressure of the original ground was the average value (final 143 kPa) of D1-D7 (D4 and D5 after 2017.1.21). The total design axial load of the four columns was 171.4 MN, which is generally consistent with the measured value. The measured load sharing ratio of the piles was 69%, compared to the design value of 75%, indicating generally reasonable agreement. In addition, level measurements confirmed that the differential settlement between the high-rise and low-rise buildings was small.

4 SEISMIC OBSERVATION

4.1 *Observed seismic events*

For seismic observation, three-component servo seismometers (accelerometers) are installed both underground (at GL-1.5 m, GL-20 m, and GL-45 m) and within the building (WT: 36F, 30F, B2F; LB: B2F; ET: 17F, B2F). The seismometer at GL-45 m is used as a trigger, with a trigger level of 0.6 cm/s² and a resolution of 6000 cm/s² / 24-bit = 3.6×10^{-4} cm/s². Some of the instruments used for static observation are connected to a dynamic amplifier, allowing the foundation behavior to be measured simultaneously at a sampling frequency of 100 Hz.

Seismic observation began in January 2017, and approximately 60 seismic events had been recorded by May 2025. The main observed events are listed in Table 1. Figure 10 shows the locations of both the monitored building and the epicenters of relatively large earthquakes. This paper focuses on the seismic events that occurred on October 7, 2018, and January 1, 2024.

Figures 11 shows observed peak accelerations of the ground and WT building. The peak accelerations at GL-20m and GL-1.5m are almost proportional to those at GL-45m. The peak accelerations at GL-1.5m are about 4 times larger than those at GL-45m, whereas the peak accelerations at GL-20 m are not as large. On the other hand, the response of the upper part of the building does not necessarily correlate proportionally with the acceleration at B2F; there are cases where the upper response is large even if the acceleration at the foundation is small. For example, during the Eastern Aichi Prefecture earthquake (M5.0) on October 7, 2018, which occurred nearby, the NS component produced a peak acceleration of 58.2 cm/s² on the ground surface (GL-1.5 m), which decreased to 16.6 cm/s² at the base floor (B2F) and further decreased to 8.3 cm/s² (average at two points on the 36th floor). In contrast, for the distant Noto Peninsula Earthquake (M7.6) on January 1, 2024, although the NS component produced a peak acceleration of 15.2 cm/s² on the ground surface (GL-1.5 m), it was almost the same at 11.7 cm/s² on B2F, and increased to 51.2 cm/s² at the 36th floor.

Table 1. Observed main events.

Occurrence at (JST)	Region name	Magnitude (M)	Depth (km)
2017/6/25 7:02:15	Southern Nagano Prefecture	5.6	7
2018/6/18 7:58:34	Northern Osaka Prefecture	6.1	13
2018/10/7 10:14:19	Eastern Aich Prefecture	5.0	42
2019/3/9 1:08:3	Cetnral and western Mino, Gifu Prefecture	4.4	42
2020/10/19 3:27:59	Cetnral and western Mino, Gifu prefecture	4.1	42
2020/11/19 9:54:55	Western Aich Prefecture	3.1	62
2021/2/13 23:07:50	Off the Coast of Fukushima Prefeture	7.3	55
2022/3/16 23:36:32	Off the Coast of Fukushima Prefeture	7.4	57
2022/4/7 9:30:35	Eastern Aich Prefecture	4.7	11
2024/1/1 16:10:22	Noto Peninsula	7.6	16

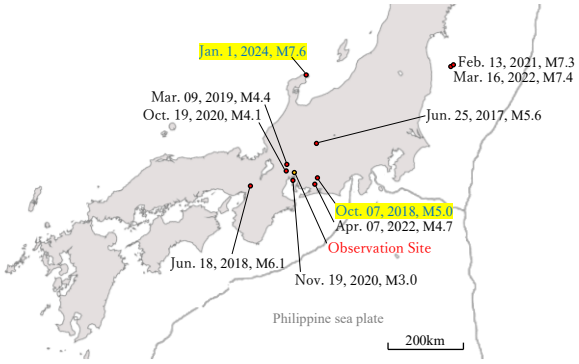

Figure 10. Observation site and epicenters of seismic

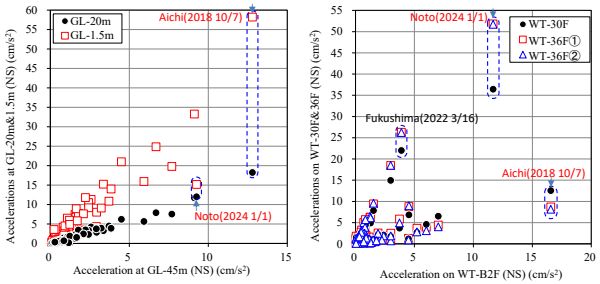

(a) Ground (NS) (b) Building (NS)

Figure 11. Observed peak accelerations in the ground and building (WT).

4.2 *Observed seismic responses of ground and superstructure*

Figures 12 shows the time histories of the measured accelerations (NS-direction) during the seismic event on January 1, 2024. The magnitude of the event is M7.6 and its epicenter is Noto Peninsula, where is far from monitored site. The acceleration at 36F is the average of two accelerometers installed on the same floor. As shown in Figure 11, the acceleration was significantly amplified at the upper floors (30F and 36F), and long-duration oscillations were observed.

Additionally, at the ground surface (GL-1.5 m), long-period components can be seen to persist beyond 100 seconds.

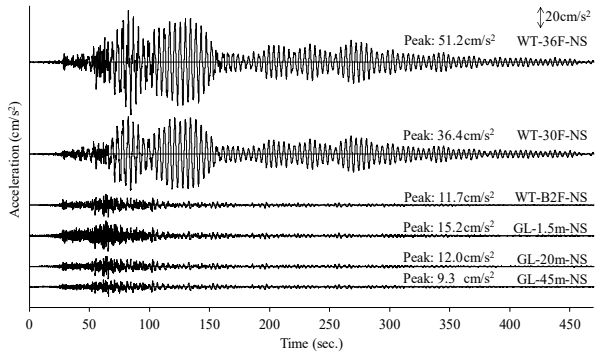

Figure 12. Acceleration time history (Noto Peninsula earthquake on January 1, 2024, NS- direction).

Figures 13 shows the time histories of the measured accelerations during the seismic event on October 7, 2018. A magnitude of the event is M5.0 and the epicenter of the event is Eastern Aichi Prefecture, where is near the monitored site. The peak acceleration at the B2F and 36F significantly decreased from that at the ground surface.

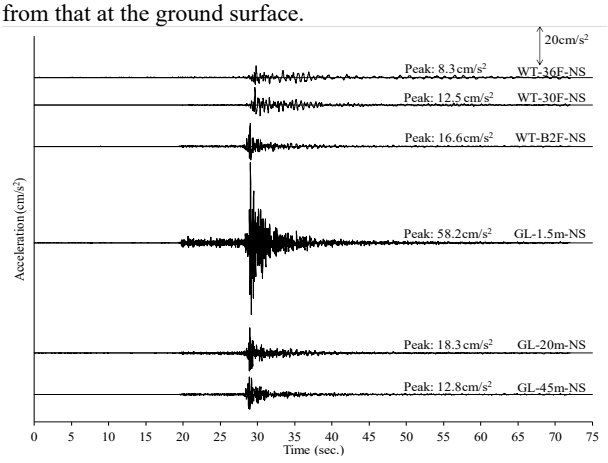

Figure 13. Acceleration time history (Eastern Aichi Prefecture earthquake on October 7, 2018, NS- direction).

Figure 14 shows the acceleration response spectrum (h = 5%) of the ground and structure motion observed during the Noto Peninsula Earthquake. From the response spectrum in the ground (GL-45m, -20 m, -1.5 m), it can be seen that the dominant periodic component of the ground motion is around 0.2 and 1 to 5 seconds, and that the long-period component is included. In particular, there is a component of less than 4 seconds, which corresponds to the predominant period of 3.5 to 4.0 seconds in the central part of the plain due to the underground structure of the Nobi Plain (Ise Bay in the south and surrounded by mountains on the other 3 sides). The natural period of the ground shallower than GL-45m can be confirmed to be approximately 0.7 seconds. This is derived from the comparison of the acceleration response spectra of GL-1.5 m (GL-20 m) and GL-45 m, as well as the Fourier spectral ratio analysis. This value corresponds to the natural period of 4H/Vs = 4×45 m / 260 m/s^2 = about 0.7 seconds estimated from the Shear wave velocity structure. The natural period of the WT is 4 seconds, and it can be seen that it is greatly amplified at 30F and 36F.

Figure 15 shows those during the Eastern Aichi Prefecture Earthquake. It can be clearly seen that the short-period component is the predominant ground motion and that the

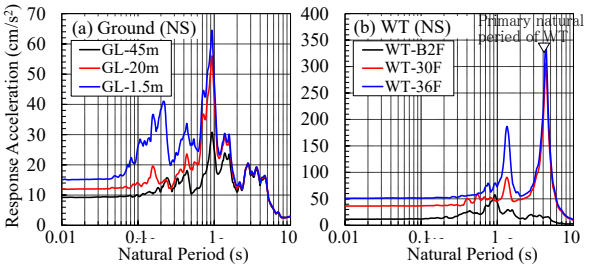

Figure 14. Acceleration response spectrum (Noto Peninsula earthquake on January 1, 2024).

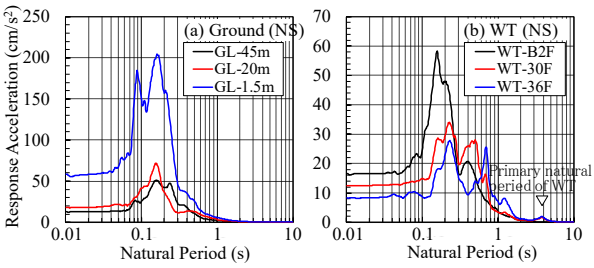

Figure 15. Acceleration response spectrum (Eastern Aichi Prefecture earthquake on October 7, 2018).

natural period component of the buildings is not input. However, it is amplified at around 3.8 seconds for WT, showing the effect of the natural period of the building.

4.3 *Observed seismic response of piled raft foundation*

Figure 16 shows the relationship between the peak acceleration observed at B2F and 30F of WT and the peak strain at the pile head of P1 (incremental strain during earthquake). In the nearby Eastern Aichi Prefecture Earthquake, the peak strain of the pile was only 7μ (P1-1 S), despite the large acceleration observed at B2F. In contrast, during the distant Noto Peninsula Earthquake, the peak strain of the pile was 32μ (P1-1 N), even though the acceleration at B2F was small. This difference in foundation behavior between the near and far earthquakes also observed in another building record (Hamada et al. 2019).

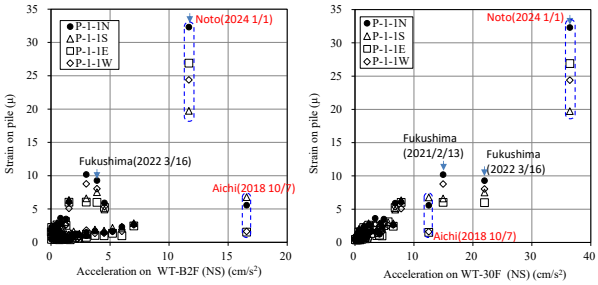

(a) Relationship with B2F (b) Relationship with 30F

Figure 16. Peak pile's strain.

Figure 17 shows the relationship between the peak acceleration observed at B2F and 30F of WT, and the peak earth pressure beneath the raft (i.e., incremental earth pressure during earthquake). A similar trend was observed in the peak strain of the pile, which correlated more strongly with the peak acceleration at 30F than at B2F. For many events, the earth pressure values recorded by the gauges installed on the DMWs (D8, D11, D13) were higher than those recorded on the original ground (D4, D5). However, during the October 7, 2018, Eastern Aichi Prefecture Earthquake, the earth pressure at D4 on the original ground was the highest. The long-term earth pressures of D8 and D4 were about 120.4 kPa and 132.6 kPa, respectively, and the incremental earth pressures during the earthquake were up to 4.68 kPa and 1.18 kPa.

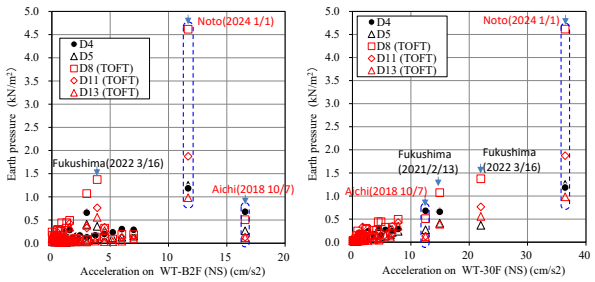

(a) Relationship with B2F (b) Relationship with 30F

Figure 17. Peak earth pressure.

4.4 *Input loss*

Figure 18 shows the Fourier spectral ratio of B2F (WT) and GL-1.5m (smoothed with a Parzen window bandwidth of 0.1 Hz). It can be clearly seen that the response factor decreases for high-frequency components above 3 Hz.

Figure 19 shows the acceleration time history of the ground surface (GL-1.5 m) and B2F observed in the Eastern Aichi Prefecture earthquake. It can be confirmed that high-frequency seismic waves predominate in GL-1.5m and are greatly attenuated in B2F. In addition, it can be confirmed that acceleration of B2F at WT (West Building), LB (Lower Building), and ET (East Building) oscillates almost similarly.

Figure 20 shows the relationship between acceleration of GL-1.5m and B2F comparing the Noto Peninsula earthquake and the Eastern Aichi Prefecture earthquake. During the Noto Peninsula earthquake, which is a distant earthquake, GL-1.5m and B2F oscillate almost similarly without any phase difference, and almost no input loss is observed. On the other hand, in the Eastern Aichi Prefecture earthquake, which is nearby earthquake, the response of B2F is remarkably reduced from that of GL-1.5m, and there is a phase difference.

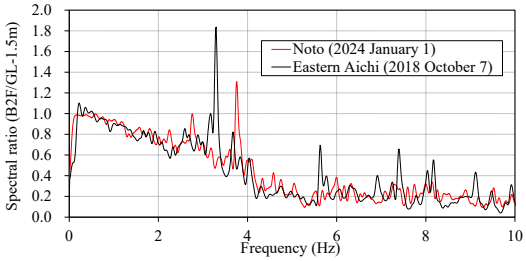

Figure 18. Fourier spectral ratio (B2F/GL-1.5m, NS-direction).

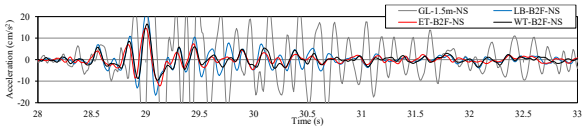

Figure 19. Acceleration time history (Eastern Aichi earthquake).

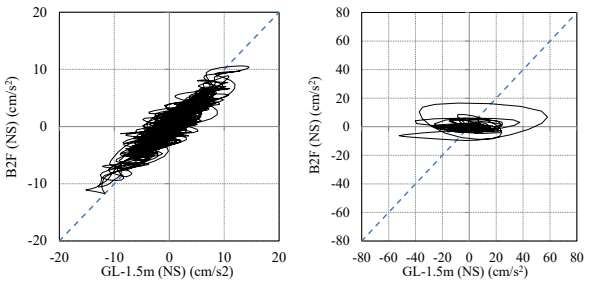

(a) Noto earthquake (b) Eastern Aichi earthquake

Figure 20. Comparison of acceleration between at GL-1.5m and B2F.

5 RELATIONSHIP BETWEEN PILE STRESS, EARTH PRESSURE AND BUILDING INERTIA FORCE

Figure 21 shows the time histories (50-150 seconds) of axial strain, bending strain of piles, and earth pressure beneath the raft observed in the Noto Peninsula Earthquake on January 1, 2024, together with acceleration and inertial force of the ground surface and the building. The axial strain is the average value (tensile: positive) of a pair of axial strains in the same section. The bending strain in the NS direction is defined as the axial strain in the N-plane minus the axial strain in the S-plane, divided by 2. Similarly, the bending strain in the EW direction is defined as the axial strain in the E-plane minus that in the W-plane, divided by 2. The acceleration of the upper part of the building, the axial strain in the pile, the bending strain in the pile, and the earth pressure beneath the raft oscillated with a natural period of 4 seconds. In addition, the axial strain measurements at Pl-1 (pile head), Pl-2 (intermediate), and P1-3 (pile toe) of the P1 pile showed almost the same values, especially between the pile head and the intermediate section. This suggests that the circumferential friction acting on the pile is relatively small, likely due to the influence of the surrounding grid-form DMWs (Hamada et al. 2020).

Focusing on Time A (130.0 seconds), the building inertia force is 17.7 MN in the east direction and -15.0 MN in the south direction, and the superstructure's inertia force is the main force. The axial strain of the pile was 19 μ (tension) in the P1 pile and -39 μ (compression) in the P4 pile, and the earth pressure (D8) was compression. The bending strain at the pile head of P1 is 8.6 μ (tensile at N-face, compressive at S-face) in the NS direction and 5.7 μ (E-face is tensile, W-face is compressive) in the EW direction. Therefore, the upper part of the building is displaced to the southeast side, which is tensile at the north and east sides of the P1 pile and compressive at the south and west sides (Fig. 22).

If an incremental axial strain of 20 μ is produced over a pile length of 32 m, the pile is stretched and compressed by 0.64 mm, and the pile core is 24 m away from the center of the building, so the pile head incremental rotation angle θ is $1/3.75\times10^{-4}$ rad. And if the caused bending strain is estimated to be 0.5~1.0 βθD (β: characteristic length of pile, D: distance between a pair of strain gauges), then $0.5\sim1.0\times1/6.25\times1/3.75\times10^{-4}$ rad×1.8 m = 3.8~7.6 μ (in case of β=l/6.25 (l/m)). It is considered that the rotation of the foundation due to the rocking motion of the building acts in the direction to cancel the pile head bending moment caused by the building inertia force by about 4~8 μ.

6 VERTICAL LOAD SHARING BETWEEN PILE AND RAFT DURING EARTHQUAKE

Figure 23 shows the relationship between the axial force of the pile, P4 and the contact earth pressure beneath the raft, D8 (DMWs). In the long-term monitoring during construction, the water pressure recovered to about 80 kPa after the deep well was stopped after construction of the raft, and the earth pressure (D8) increased from about 110 kPa to about 122 kPa while the water pressure acting on the raft remained constant. In the meantime, the axial force of the pile increased from about 15000 kN to about 23000 kN (compression: positive). According to the relationship between the axial force of the pile (P4) and the earth pressure (D8) during earthquake (Noto Peninsula Earthquake on January 1, 2024), the earth pressure also mobilized during earthquake, and the load sharing ratio between the axial force of the pile and the raft (approximately 2000kN: 4 kPa) was nearly equal to the ratio during construction (approximately 8000kN: 12 kPa).

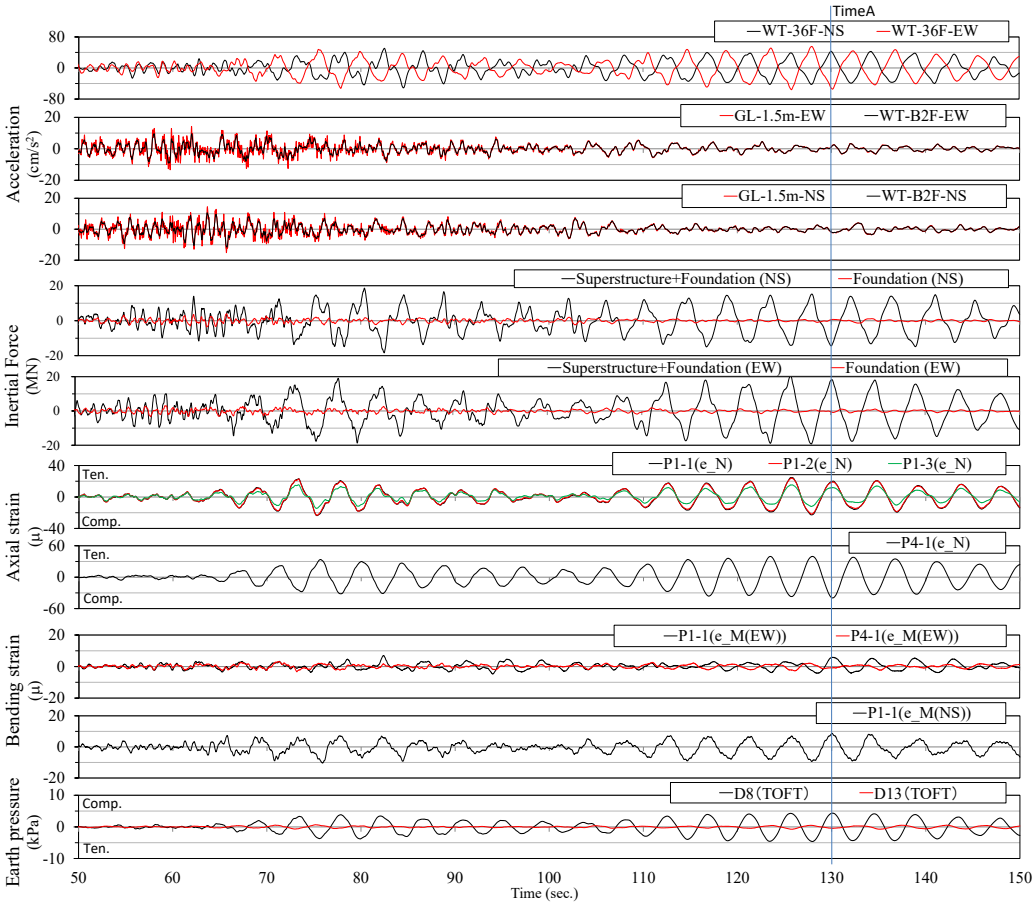

Figure 21. Time histories of axial strain, bending strain of piles and earth pressure (Noto peninsula earthquake on January 1, 2024).

7 CONCLUSIONS

The following results were obtained from the seismic observations, including those of the foundation.

For distant earthquakes with long-period input ground motions close to the natural period of the building, the foundation exhibited behavior nearly identical to that of the ground surface, indicating no significant input loss. In contrast, for nearby earthquakes with short-period motions, a large input loss was observed. It was inferred that the rotational response of the foundation, caused by the rocking motion of the superstructure, had a significant influence on the bending moments at the pile heads during earthquakes. Additionally, the vertical load-sharing ratio between the piles and the raft in response to fluctuating axial forces during the earthquakes closely corresponded to the ratio observed at the time of construction.

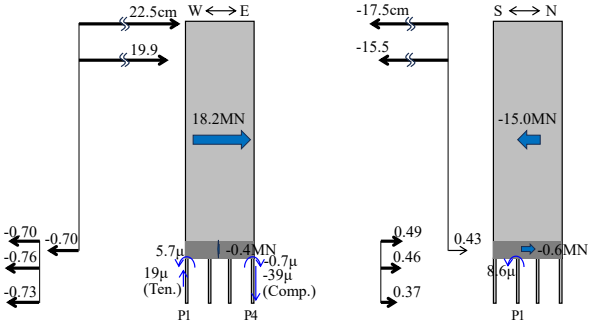

(a) EW-direction (b) NS-direction

Figure 22. Deformation of ground and structure at Time A.

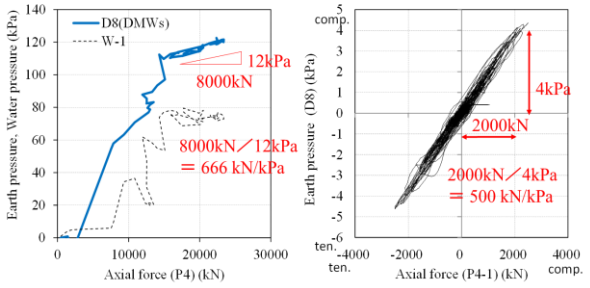

(a) During construction (b) During Noto earthquake

Figure 23. Relationship between axial load of pile and contact earth pressure beneath raft.

8 REFERENCES

Yamashita, K., Hamada, J., Onimaru, S. and Higashino, M. 2012. Seismic behavior of piled raft with ground improvement supporting a base-isolated building on soft ground in Tokyo. *Soils & Foundations*, Vol.52, No.5, 1000-1015. Special issue on Geotechnical Aspects of the 2011 off the Pacific coast of Tohoku Earthquake.

Hamada, J., Umemura, K. and Honda, T. 2024. Seismic observation of 36- and 17-story buildings connected by low-rise building foundation. *WCEE2024*.

Tanikawa, T., Hamada, J. and Honda, T. 2015. Mechanical joints transmitting lateral force to grid-form soil improvement. *15ARC*.

Hamada, J. and Yamashita, K. 2019. Seismic observations on piled raft foundation subjected to unsymmetrical earth pressure during far earthquake and near earthquake. *Geotechnical Engineering Journal of the SEAGS & AGSSEA* Vol. 50 No. 4, 5-14.

Hamada, J., Wakai, S. and Yamashita, K. 2020. Seismic observation of large-scale piled raft foundation with grid-form deep mixing walls supporting isolated office building. *17th World Conference on Earthquake Engineering*.